THE JOURNAL OF PHYSICAL CHEMISTRY B

Article

pubs.acs.org/JPCB

Dominant Stable Radicals in Irradiated Sucrose: g Tensors and Contribution to the Powder Electron Paramagnetic Resonance Spectrum

Hendrik De Cooman,[†,‡] Joke Keysabyl,[†] Jevgenij Kusakovskij,[†,§] Andy Van Yperen-De Deyne,[‡] Michel Waroquier,[‡] Freddy Callens,[†] and Henk Vrielinck[†,*]

[†]Ghent University, Department of Solid State Sciences, Electron Magnetic Resonance Research Group, Krijgslaan 281-S1, B-9000 Ghent, Belgium

[‡]Ghent University, Center for Molecular Modeling, Technologiepark 903, B-9052 Zwijnaarde, Belgium

[§]Vilnius University, Institute of Applied Research, Sauletekio av. 9-III, LT-10222 Vilnius, Lithuania

Supporting Information

ABSTRACT: Ionizing radiation induces a composite, multiline electron paramagnetic resonance (EPR) spectrum in sucrose, that is stable at room temperature and whose intensity is indicative of the radiation dose. Recently, the three radicals which dominate this spectrum were identified and their proton hyperfine tensors were accurately determined. Understanding the powder EPR spectrum of irradiated sucrose, however, also requires an accurate knowledge of the **g** tensors of these radicals. We extracted these tensors from angular dependent electron nuclear double resonance-induced EPR measurements at 110 K and 34 GHz. Powder spectrum simulations using this completed set of spin Hamiltonian parameters are in good agreement with experimentally recorded spectra in a wide temperature and frequency range. However, as-yet nonidentified radicals also contribute to the EPR spectra of irradiated sucrose in a non-negligible way.

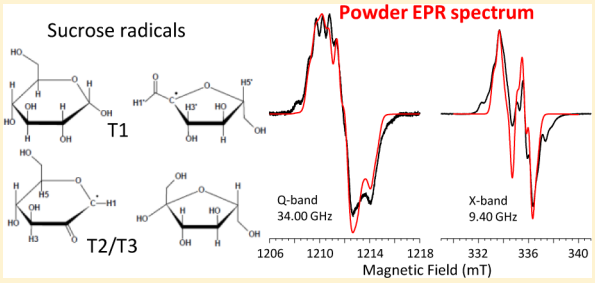

1. INTRODUCTION

The structure of radiation-induced radicals in solid state sucrose has been studied with electron magnetic resonance (EMR) techniques, electron paramagnetic resonance (EPR) in particular, since the early sixties of the 20th century.[1−6] However, only recently has the identity of three radicals (T1−T3), which appear to have a dominant contribution to the room temperature (RT) stable EPR spectrum of irradiated sucrose, been convincingly established via comparison of proton hyperfine (HF) interactions, determined from single crystal electron nuclear double resonance (ENDOR) experiments, with the results of high-level density functional theory (DFT) calculations.[7−9] Figure 1 shows the intact sucrose molecule along with the models for these dominant radicals. T1 has the unpaired electron mainly localized at carbon atom C2′ in the fructose unit. The EMR properties of T2 and T3 are very similar, and hence, they are believed to have basically the same radical structure, in slightly different conformations. They have their main unpaired electron density at C1 in the glucose unit. The formation of all three radicals involves scission of the glycosidic bond between the rings. Moreover, the carbon atom bearing the main unpaired electron density is located next to the ring oxygen and has a carbonyl group at a β-carbon position. These radical structures differ strongly from the intact sucrose molecule and most probably have a complex multistep formation mechanism. In contrast, the (at RT) highly unstable radicals produced by irradiation at 10 K are formed by simple H-abstraction at C or O atoms.[10]

There are two main motivations for studying these radicals. The first is mostly fundamental: elucidating the complex radiation chemistry of carbohydrates, and more specifically understanding the role of sugar radicals in the radiation damage to complex biomolecules such as DNA. In this context, the glycosidic bond scission in the stable radicals in sucrose, also observed for the dominant metastable radical in glucose 1-phosphate,[11,12] is remarkable and supports the idea that sugar radicals are precursors for strand breaks in DNA.[13]

A second motivation springs from the fact that ionizing radiation induces stable radicals in sugars, whose EPR signal intensity may be applied to determine the radiation dose. Since the beginning of the 1980s, the potential of sucrose in radiation dosimetry has been recognized,[14,15] and it has been the subject of many EPR studies since then.[16−22] When samples are properly stored, the EPR spectrum of irradiated sucrose has long-term stability, and after a short initial period of strong changes[20,23] it shows only limited fading. Sucrose exhibits a radiation sensitivity similar to that of alanine but a smaller linear dose range. Table sugar consists of over 90% sucrose. The

Received: January 3, 2013
Revised: May 23, 2013

   dx.doi.org/10.1021/jp400053h | J. Phys. Chem. B XXXX, XXX, XXX−XXX

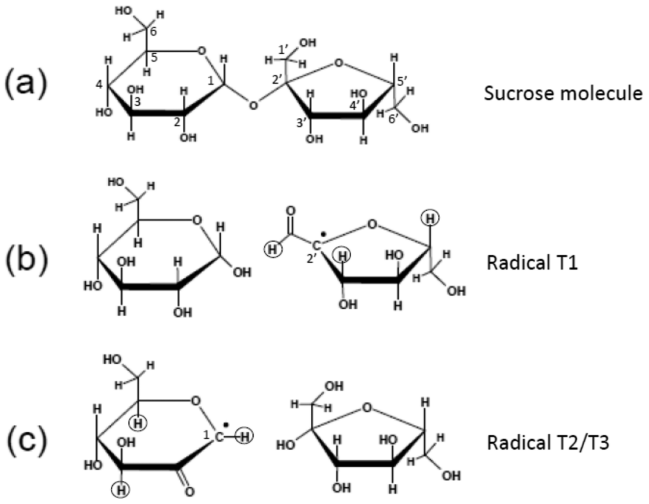

Figure 1. Intact sucrose molecule with IUPAC atomic labeling (a) and models for the RT stable radicals T1 (b) and T2/T3 (c), as determined from comparison with DFT calculated ^{1}H HF tensors.[8,9] The carbon positions bearing the main spin density, C2′ in the fructose unit for T1, and C1 in the glucose unit for T2−T3, are indicated in the radical structures with ●. The ^{1}H nuclei whose HF interaction is resolved in the EPR and/or ENDOR spectra in the two radical models are circled.

radiation-induced EPR spectra of these materials resemble each other very closely. For this reason, table sugar seems particularly interesting for accident and emergency dosimetry. The composite nature of the stable EPR spectrum of irradiated sucrose, as a result of the formation of various types of radicals,[21] along with the complex transformations of this spectrum a short time after irradiation,[20,23] are issues of concern. In the same context, one can apply EPR spectrometry for detection and control of irradiated sugar-containing foodstuffs.[24−27] An additional complication arises here: in foodstuffs, usually a mixture of sugars is present, all giving rise to different radiation-induced EPR spectra. In this respect, a detailed understanding of the shape of the powder EPR spectrum of various irradiated common sugars is very relevant, and this study aims to contribute to understanding the spectrum of irradiated sucrose.

Following the recent thorough characterization and identification of three dominant, RT stable radicals in sucrose,[7−9] one may easily presume that the powder EPR spectrum of irradiated table sugar is understood to a large extent. Reliable powder pattern simulations, however, also require knowledge of the **g** tensors for the radicals, whose anisotropy is expected to be considerable because of delocalization of the unpaired electron onto the β-carbonyl and ring oxygen.[4,8,9] Attempts have been made to determine these tensors experimentally from the angular dependence of the Q-band EPR spectra on single crystals recorded at RT, but due to the compositeness of the spectra, this allowed determination of the **g** tensor for only one of the radicals.[4] In a later study,[6] the **g** tensors of the radicals were extracted via simulation of the powder EPR spectra in four microwave frequency bands (9.7−285 GHz), using the HF tensors determined in a low-temperature (55 K) ENDOR study.[5] A more recent ENDOR study[7] of our group at 110 K demonstrated that the HF tensors determined by Vanhaelewyn et al.[5] needed substantial correction, casting also doubt on the analysis of the high-frequency powder EPR spectra. In the present study we determine the **g** tensors of the three dominant RT stable radicals using ENDOR-induced EPR (EIE)[28] for separating the EPR spectra of different types of radicals. The methodology is similar to that in the pioneering EIE work of Kang et al. on determining the **g** tensors for radicals in malonic acid and guanine hydrochloride dehydrate.[29] The obtained **g** tensors are compared to those from the previous studies and to results of periodic DFT calculations on the known models for these radicals (Figure 1). Afterward, having the **g** tensors at hand, powder EPR simulations at X- and Q-band frequencies (9.5 and 34 GHz, respectively) are compared with experimental spectra. Interestingly, the statistical decomposition of the EPR spectrum of irradiated sucrose yielded up to six distinct components, three of which were clearly dominant.[5] In support of this finding, we show that certain features of the powder EPR spectra are not covered by the simulations of the known radicals.

2. EXPERIMENTAL AND COMPUTATIONAL METHODS

A. Experimental Details. Sucrose single crystals were grown from saturated aqueous solutions in our laboratory.[7] Powders were either obtained directly (Sigma Aldrich) or obtained by crushing single crystals. Sucrose crystals are monoclinic with space group $P2_1$ and two symmetry related molecules (= sites) in the unit cell, transformed into one another by a 2-fold screw-rotation around the $\langle b\rangle$ axis.[30] The lattice parameters are a = 1.0868 nm, b = 0.8710 nm, c = 0.7761 nm, and β = 102.97°, with β the angle between the $\langle a\rangle$- and $\langle c\rangle$-axes. Sucrose powders and single crystals were X-ray irradiated at RT to a dose in the range 10−100 kGy using a Philips tungsten anticathode X-ray tube operated at 60 kV and 40 mA. The crystals were subsequently oriented by X-ray diffraction (pole figures) with a Bruker D8 diffractometer, transferred and glued to quartz sample rods to allow sample rotation in the magnetic field around the $\langle a^*\rangle$ (perpendicular to $\langle b\rangle$ and $\langle c\rangle$), $\langle b\rangle$, and $\langle c\rangle$ axes.

Q-band EPR, ENDOR, and EIE spectra were recorded using a continuous wave Bruker ElexSys E500 spectrometer, equipped with an Oxford CF935 He-flow cryostat (2−300 K), a Pendulum CNT-90XL frequency counter, and a Bruker ER 035 NMR Gaussmeter. The magnetic fields were calibrated against the $g_\perp$ component of a CO_3^{3-} radical in irradiated calcite powder ($g_\perp$ = 2.0031).[31] X-band powder EPR spectra were recorded using a Bruker ESP300E setup, fitted to an Oxford ESR-900 cryostat, equipped with a HP-5350 frequency counter and a Bruker ER 035 NMR Gaussmeter. For field calibration in X-band, the spectrum of diphenyl picryl hydrazyl (DPPH, g = 2.0036) was measured. All presented X- and Q-band EPR spectra have been normalized to 9.40 and 34.00 GHz, respectively, and were recorded at low microwave power (<100 μW) and low modulation frequency (1−3 kHz), in order to avoid distortion of the spectra.

The spectra were interpreted using the standard spin Hamiltonian[28] for a paramagnetic center with $S = {}^1/_2$ interacting with nuclei with $I = {}^1/_2$ (protons, ^{1}H)

$$\hat{H}_S = \mu_B \vec{B}\cdot\vec{\vec{g}}\cdot\hat{\vec{S}} + \sum_k (\hat{\vec{S}}\cdot\vec{\vec{A}}^k\cdot\hat{\vec{I}}^k - g_N\vec{B}\cdot\hat{\vec{I}}^k) \quad (1)$$

in which the symbols have their usual meaning, with g_N referring to the proton nuclear g factor. In agreement with our previous studies on sucrose, $\langle a^*\rangle$, $\langle b\rangle$, and $\langle c\rangle$ are chosen as orthogonal reference system for representation of the **g** and HF tensors. The actual rotation planes in the angular

dx.doi.org/10.1021/jp400053h | J. Phys. Chem. B XXXX, XXX, XXX−XXX

dependent EIE study (see caption of Figure 2) were accurately determined by simultaneously fitting the angular variations of

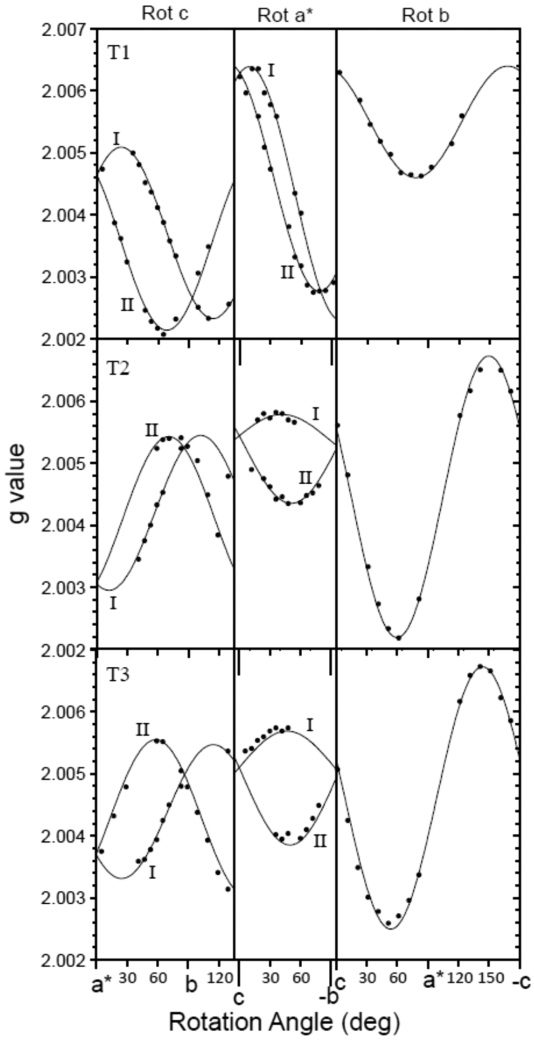

Figure 2. EIE angular variation of the stable radicals T1, T2, and T3 in X-irradiated sucrose, recorded at Q-band and 110 K (symbols), and simulations using the **g** tensor presented in Table 1 (I) and the symmetry-related tensor (II) by applying a 180° rotation around the ⟨*b*⟩ axis (full lines). In the (ca*) rotation plane (rot b), the spectra of the two symmetry related sites coincide. The rotation planes were slightly misaligned. The polar angles of the actual rotation planes, determined by fitting the ENDOR angular dependence, for the rot ⟨*c*⟩, rot ⟨*a**⟩, and rot ⟨*b*⟩ data were $\theta = -6°$, $\phi = -48°$; $\theta = 92°$, $\phi = 7°$; and $\theta = 91°$, $\phi = 94°$, respectively.

the ENDOR spectra for the largest HF coupling for each radical ($H_{\beta 1}$(T1), H_{α}(T2), and H_{α}(T3)), using the previously determined HF tensors for the stable radicals in sucrose[7,9] (see Table S1 in the Supporting Information). All single crystal and powder EPR and ENDOR spectra were simulated by full diagonalization of the spin Hamiltonian (1) using the EasySpin libraries[32] in Matlab.

B. Computational Details. All calculations were made with the CP2K program package[33] in a periodic approach using a super cell, consisting of two sucrose crystallographic unit cells along the *c* axis (four sucrose molecules, one of which having the radical structure, 179 atoms in total) as the periodic unit. Geometry optimizations were first made using the Gaussian and plane-waves (GPW) method[34] with a plane-wave cutoff of 320 Ry, TZV2P GTH basis sets, and GTH pseudopotentials.[35,36] Subsequently, geometries were further optimized in an all-electron approach using the Gaussian-augmented plane-wave (GAPW) method[37] with a plane-wave cutoff of 250 Ry and TZV2P basis sets.[38] The **g** tensor calculations[39] were also performed using the GAPW method, with the same basis set and plane-wave cutoff, while the theoretical HFC tensors[40] were calculated in previous work.[9] A BLYP functional[41,42] was employed for all calculations. This method has been validated for ^{1}H HF tensor calculations in similar work on sucrose and has the advantage of including the environment in a more natural way compared to cluster calculations.[43] However, for **g** tensor calculations it has been shown by Neese et al.[44] and by Van Yperen-De Deyne et al.[45] that effective potential (V_{eff}) methods[46] fail in describing the exchange contribution of the two-electron spin−orbit interaction. The effective spin−orbit interaction includes the gradient of the exchange correlation functional v_{xc}, and it has first been demonstrated by Neese that this ∇v_{xc} term yields a contribution of approximately the same magnitude but with opposite sign compared to the exact exchange as calculated in the spin−orbit mean field (SOMF) approach, as implemented in ORCA. This shortcoming is circumvented by introducing a scaling approximation, where the small underestimated spin-other-orbit corrections were also taken into consideration. This issue has also been intensively investigated by Van Yperen-De Deyne et al., and the periodic CP2K code has been adapted in view of this scaling method (with a scaling factor $\sigma' = -2.8$), bringing the periodic DFT predictions close to SOMF and similar methods, available in nonperiodic codes.[44,47,48]

3. RESULTS AND DISCUSSION

A. Single Crystal EIE Study at 110 K. In order to extract the **g** tensors of the radicals T1, T2, and T3, we followed a procedure similar to that in ref 29, as outlined in Figures 2 and 3 of ref 49. EIE spectra were recorded at 110 K, the temperature at which our earlier ENDOR studies were conducted, monitoring the intensity of the $H_{\beta 1}$ proton coupling for T1 and the H_{α} coupling for T2 and T3 as a function of magnetic field strength in three rotation planes, where possible for the two symmetry related sites. Q-band ENDOR spectra at RT exhibited too low signal-to-noise ratio for recording EIE spectra. For EIE spectra that exhibited an approximately symmetric HF structure, the center of the pattern was used as data point. The combined error of determining this center and of possible differences between HF patterns recorded with EIE and EPR, due to the strongly different conditions of saturation in the two types of experiments, is estimated to be smaller than 0.15 mT ($\sim 2 \times 10^{-4}$ in *g* value). The **g** tensors were then determined by least-squares error fitting of calculated resonance field positions from the first term in the spin Hamiltonian (1) to the experimental data. The best-fit principal *g* values and directions are listed in Table 1. The results of experiments and fittings are summarized in Figure 2: the final simulations match experiments very well, with root-mean-square errors of 6×10^{-5}, 7×10^{-5}, and 1×10^{-4} for T1, T2, and T3, respectively. For all three radicals, one principal *g* value is very close to g_e while the other two exhibit considerable positive shifts, as expected for carbon-centered radicals with delocalization of the unpaired electron onto (carbonyl and ring) oxygen. Similar shifts have been observed and reproduced by DFT calculations for semiquinone and tyrosyl radicals, whereas glycyl radicals,

dx.doi.org/10.1021/jp400053h | J. Phys. Chem. B XXXX, XXX, XXX−XXX

Table 1. g Tensors Determined from EIE Experiments at 110 K for T1−T3 in Irradiated Sucrose, Compared with Literature and DFT Results, Represented in the ⟨a*⟩, ⟨b⟩, ⟨c⟩ Crystal Reference Frame and All Related to the Same Site (I)[a]

		g	δg		δg*	⟨a*⟩	⟨b⟩	⟨c⟩	Δ
					Radical T1				
exp[b]	1	2.0021	−0.2	Iso.	2.23	0.3619	−0.9232	−0.1295	
	2	2.0049	2.6	Ax.	2.43	0.8781	0.2909	0.3798	
	3	2.0066	4.3	Rh.	0.70	−0.3130	−0.2512	0.9160	
exp[c] not analyzed									
exp[d]	1	2.00197	−0.33	Iso.	2.10				
	2	2.00466	2.36	Ax.	2.43				
	3	2.00658	4.28	Rh.	0.79				
DFT[b]	1	2.00232	0.002	Iso.	2.02	0.4612	−0.8855	−0.0560	7.4
	2	2.00458	2.260	Ax.	2.02	0.8244	0.4043	0.3962	7.3
	3	2.00612	3.802	Rh.	0.76	−0.3282	−0.2289	0.9165	1.4
					Radical T2				
exp[b]	1	2.0020	−0.3	Iso.	2.40	0.8367	−0.2505	0.4871	
	2	2.0054	3.1	Ax.	2.70	0.3042	0.9521	−0.0328	
	3	2.0067	4.4	Rh.	0.48	−0.4555	0.1756	0.8728	
exp[c]	1	2.0027	0.4	Iso.	2.47	0.882	0.187	0.435	25
	2	2.0049	2.6	Ax.	2.07	0.022	0.902	−0.432	28
	3	2.0067	4.4	Rh.	0.87	−0.472	0.391	0.790	13
exp[d]	1	2.00180	−0.50	Iso.	1.90				
	2	2.00400	1.70	Ax.	2.40				
	3	2.00680	4.50	Rh.	1.17				
DFT[b]	1	2.00212	−0.192	Iso.	2.08	0.8024	−0.2174	0.5557	4.8
	2	2.00498	2.659	Ax.	2.27	0.2645	0.9644	−0.0047	2.8
	3	2.00609	3.774	Rh.	0.49	−0.5349	0.1508	0.8313	5.3
					Radical T3				
exp[b]	1	2.0020	−0.3	Iso.	2.43	0.7428	−0.3772	0.5532	
	2	2.0055	3.2	Ax.	2.73	0.3363	0.9246	0.1790	
	3	2.0067	4.4	Rh.	0.44	−0.5790	0.0531	0.8136	
exp[c]	1	2.0027	0.4	Iso.	2.47	0.882	0.187	0.435	34
	2	2.0049	2.6	Ax.	2.07	0.022	0.902	−0.432	40
	3	2.0067	4.4	Rh.	0.87	−0.472	0.391	0.790	20
exp[d]	1	2.00200	−0.30	Iso.	2.12				
	2	2.00524	2.94	Ax.	2.42				
	3	2.00603	3.73	Rh.	0.33				
DFT[b]	1	2.00212	−0.192	Iso.	2.08	0.8024	−0.2174	0.5557	9.8
	2	2.00498	2.659	Ax.	2.27	0.2645	0.9644	−0.0047	11.5
	3	2.00609	3.774	Rh.	0.49	−0.5349	0.1508	0.8313	6.2

[a]Errors on the experimental principal values are estimated at ±0.0002 and ±0.0100 for the direction cosines. δg values are given in parts per thousand and angles between principal directions, Δ, in degrees, relative to our experimental results. [b]This study. [c]Reference 4. [d]Reference 6.

where delocalization onto neighboring oxygen is absent, do not exhibit such shifts.[50−53]

It is worth noting that the procedure followed here implicitly eliminates Schonland ambiguity,[54,55] which refers to the fact the **g** or **A** tensor fitting result of angular dependent EPR and ENDOR data, respectively, in three rotation planes may not be unique. In many cases, two tensors with distinct principal values and directions fit the data in these planes equally well, but only one of them—the actual tensor to be determined—also reproduces the angular variation outside these three planes. The origin of this ambiguity is an ambiguity in the crystal rotation sense. For crystals exhibiting monoclinic or orthorhombic symmetry, this is related to the site assignation in the rotation planes. In our previous studies of these centers, we solved the Schonland ambiguity for the HF tensors by measurements in additional rotation planes.[7,9] Hence, simulations allow assigning each branch of ENDOR transitions in each rotation plane unambiguously to one of the two sites, leaving no ambiguity in the assignation of the corresponding branches in the EIE angular dependences. The **g** and HF tensors corresponding to the largest coupling for each of these radicals are thus unambiguously related and refer to the same site. A site ambiguity remains for the smaller couplings, as will be discussed further on.

Figure 3 shows the experimental EIE spectra recorded for magnetic field orientations close to the ⟨a*⟩, ⟨b⟩, and ⟨c⟩ directions, along with simulated EPR HF patterns for the three radicals, using the **g** tensor data in Table 1 and the HF tensors in Table S1 of the Supporting Information. The overall agreement is very good, especially for the peak positions. It is not so surprising that EIE spectra do not perfectly reproduce the relative EPR line intensities of the simulations, as possible nonlinear effects of the magnetic field strength on the ENDOR frequencies are not considered in this technique. In addition, EPR and ENDOR signal intensities are governed by strongly different relaxation mechanisms, which may produce differences in line shapes as well.

dx.doi.org/10.1021/jp400053h | J. Phys. Chem. B XXXX, XXX, XXX−XXX

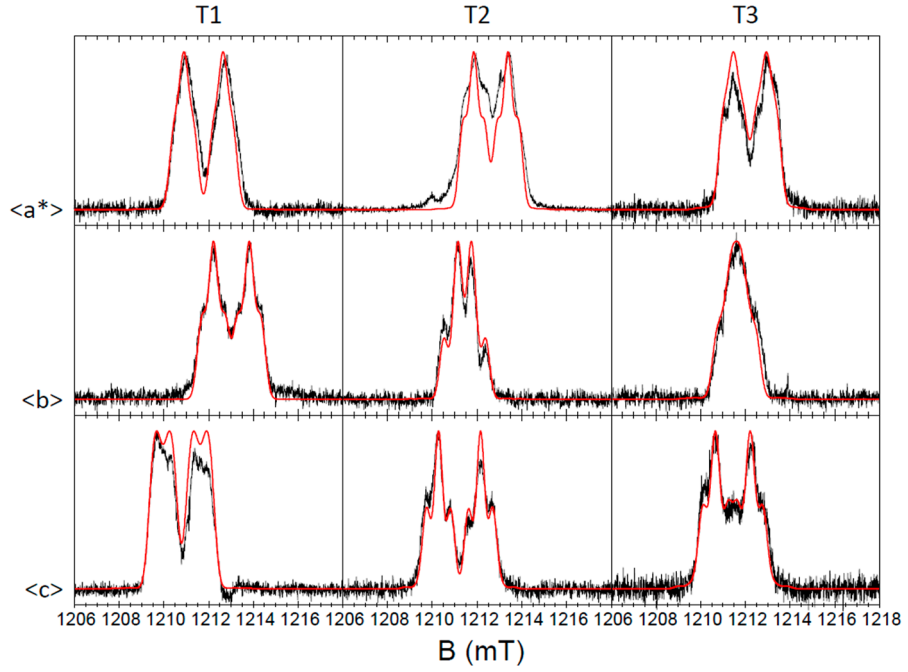

Figure 3. Comparison between experimental (black) and simulated (red) Q-band (34.00 GHz) single crystal EIE spectra in the ⟨*a**⟩, ⟨*b*⟩, and ⟨*c*⟩ crystal orientations. Simulations were performed using the **g** tensor data in Table 1 and the HF tensor data for three ^{1}H nuclei of each radical in Table S1. An isotropic residual line width of 0.48 mT has been used for the simulations.

Simulations for other orientations in the three rotation planes, displayed in Figure S1 of the Supporting Information, also lead to very convincing agreement, proving the validity of our **g** tensor analysis. Because also the smaller HF couplings are resolved, it is important for the simulations of these angular dependent spectra—and for simulations of powder spectra further on—that the **g** and all HF tensors refer to the same site. This connection between the tensors may in principle be established experimentally via EIE measurements on ENDOR lines of the smaller couplings or via General Triple spectroscopy,[28] but we have not systematically performed such experiments. We made the connection here via comparison with DFT calculations for the radicals,[8,9] which directly yield tensors related to the same site. The agreement between DFT calculated (see refs 8 and 9) and experimental HF tensors in Table S1 is so good that this can be done unambiguously. On some of the tensors published in refs 7 and 9, a symmetry transformation corresponding to a rotation over 180° around the ⟨*b*⟩ axis has been applied in order to match the DFT calculated direction cosines. We also verified that the combinations of tensors in Table S1 produce the best agreement between experimental EIE and simulated EPR spectra (see Figure S1).

In the EIE angular dependence of radical T2, for certain orientations in the (*bc*) plane (site II around 50°, e.g.), a fourth HF splitting appears to be resolved, which could not be extracted from the ENDOR analysis.[7] Very probably, this splitting corresponds to a smaller ^{1}H interaction of a more distant proton. DFT calculations (results not shown) indicate that the coupling with one of the protons hydrogen-bound to the radical may have the right order of magnitude. The presence of this extra splitting has little influence on determining the HF pattern centers, which are very well reproduced by the simulations.

B. Comparison with Earlier Literature Results and DFT Calculations of the g Tensors. In Table 1 our results for the **g** tensors are compared with those reported in the literature. Sagstuen et al. determined the **g** tensor for one of the radicals, deduced from Q-band EPR measurements on single crystals at RT.[4] Georgieva et al. determined **g** tensors for all three dominant radicals from multifrequency powder EPR measurements at variable temperature.[6] Principal directions are compared by calculating the angles Δ between corresponding direction cosines (always referred to our present experimental results). More than on absolute principal values, we focus on the deviations (δg, expressed in parts per thousand) from the free electron *g* value (g_e = 2.0023) and properties derived from these: the isotropic shift $\delta g_{iso} = (\delta g_1 + \delta g_2 + \delta g_3)/3$, the axial parameter $\delta g_{ax} = (\delta g_2 + \delta g_3)/3 - 2\delta g_1/3$, and the relative rhombicity $(\delta g_3 - \delta g_2)/\delta g_{ax}$, as for the three **g** tensors we determined $g_e \approx g_1 \ll g_2 < g_3$.

The comparison with the results of Sagstuen et al.[4] is most straightforward. As explained in ref 7, the radical for which the **g** tensor is determined in that paper most probably corresponds to T3, and certainly not to T1. Hence, we compare it here with T2 and T3. As in ref 8, a correction in the sign of certain principal direction cosines of the **g** tensor is applied before comparison with our present results. There is an obvious good agreement between the principal values of the tensors in the two studies, although the tensor we determined appears to be slightly more axial and considerably less rhombic than that earlier reported. The difference in the principal directions is more substantial. The agreement seems best with T2, but this may be fortuitous. The most plausible reason for this discrepancy is that determining the **g** tensor, especially its principal directions, from angular dependent composite EPR spectra is obviously more subject to errors than using EIE, where contributions of distinct radicals are isolated. A second source of discrepancy may be a previously reported slight temperature dependence of the spin Hamiltonian parameters of these radicals.[7] However, neither the single crystal spectra in the ⟨*a**⟩, ⟨*b*⟩, and ⟨*c*⟩ directions (see section 3.C and Figure 4)

dx.doi.org/10.1021/jp400053h | J. Phys. Chem. B XXXX, XXX, XXX−XXX

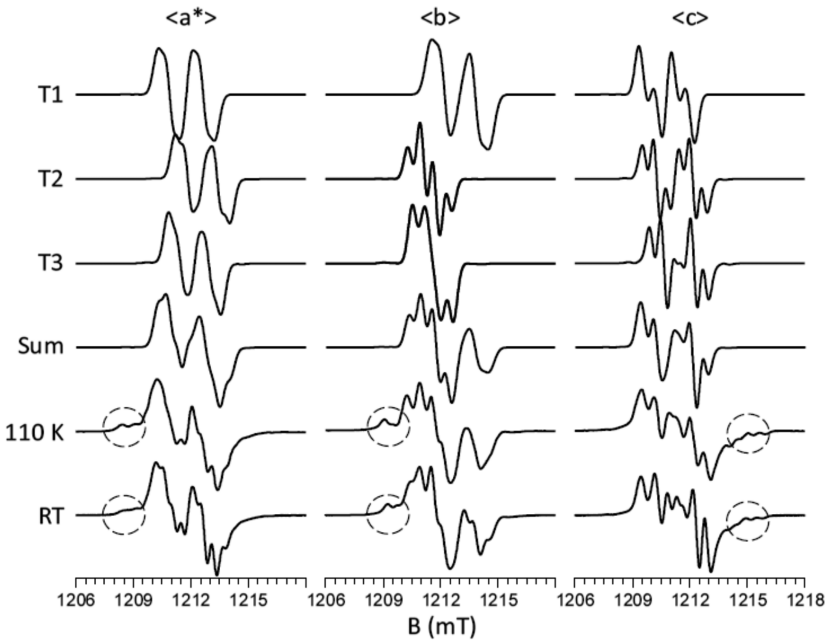

Figure 4. Comparison between experimental (recorded at 110 K and RT, modulation frequency 3 kHz, microwave power 9 μW at 110 K and 90 μW at RT) and simulated Q-band (34.00 GHz) single crystal EPR spectra in the $\langle a^* \rangle$, $\langle b \rangle$, and $\langle c \rangle$ crystal orientations. Simulations were performed using the **g** tensor data in Table 1 and HF tensor data for three ^{1}H nuclei of each radical in Table S1. The individual radical contributions are given anisotropic line widths with principal directions along the $\langle a^* \rangle$, $\langle b \rangle$, and $\langle c \rangle$ axes and principal values for T1: [17, 20, 15] MHz, and T2 and T3: [17, 16, 15] MHz. In the sum spectra T1:T2:T3 intensity ratios of 1:0.72:0.48 have been used. These values were determined via optimization of the agreement between simulated and experimental spectra by visual inspection.

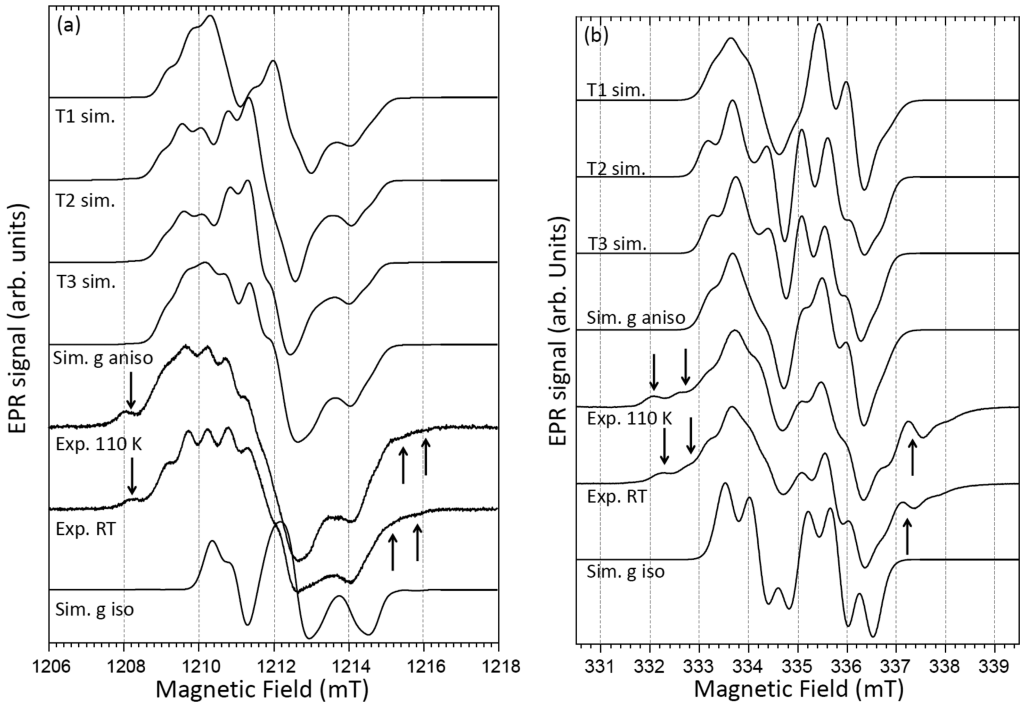

Figure 5. Q-band (a) and X-band (b) experimental powder EPR spectra at 110 K and RT, and simulations. In the sum spectra the three radicals have been attributed a weight ratio (T1:T2:T3) of 1:0.72:0.48, like in the single crystal. Wing lines not covered by the simulations are marked with arrows. All experimental spectra were recorded at a modulation frequency of 3 kHz. (a) Q-band spectra were normalized to 34.00 GHz and recorded at a low microwave power of 9 μW (110 K) and 90 μW (RT). For simulations, a line width tensor proportional (×0.9, close to 1) to that derived from the single crystal simulations was used. (b) X-band spectra were normalized to 9.40 GHz and recorded at low microwave powers of 20 μW (110 K) and 200 μW (RT). For the simulations a line width proportionality factor of 0.7 was used.

nor the powder spectra (see section 3D and Figure 5) exhibit significant changes in spectral line positions in the magnetic field region of the T1−T3 contribution. This strongly suggests that the temperature dependence of the **g** tensor of these radicals is very limited in the temperature range between 110 K and RT.

dx.doi.org/10.1021/jp400053h | J. Phys. Chem. B XXXX, XXX, XXX−XXX

For the comparison with the results of Georgieva et al., we first note that the principal directions of the **g** tensors in that study are only given indirectly, via the Euler angles of the proton HF tensors of ref 5 in the **g** tensor reference frame of each radical. As the relative Euler angles of the HF tensors corresponding to a single radical are not consistent between refs 6 and 5, we cannot compute a single set of principal directions for these **g** tensors. Moreover, the principal HF tensor directions in ref 5 were later on shown to need substantial correction. For these reasons, only a comparison for the principal g values seems meaningful. Despite the aforementioned inconsistencies, for radical T1 the comparison is quite favorable: the isotropic value, axiality, and rhombicity are quite similar. For T2 and T3, when only comparing absolute principal values, one might at first glance also consider the agreement fair. Closer inspection of the g shifts and derived parameters, however, shows that for T2 the rhombicity reported in ref 6 is much larger than that for our results, whereas for T3 exactly the opposite is observed. Comparing the literature tensors[6] for T2 and T3, one observes that their largest g values and rhombicities differ quite substantially from each other. One would not expect this for radicals otherwise exhibiting very similar properties and sharing the same basic structure. Indeed, the **g** tensors we determined for T2 and T3 have practically the same principal values, but slightly different principal directions, like for their three ^{1}H HF tensors. This is consistent with the viewpoint that these are two slightly different conformations of the same radical structure. This already indicates that the **g** tensors determined in this work are more reliable, although the accuracy of their principal values may be further improved by experiments at higher microwave frequencies. The use of inaccurate HF tensors and the large number of fitting parameters used in the powder EPR simulations are obvious sources of errors in ref 6.

Finally, also reported in Table 1 are the results of periodic **g** tensor calculations for the two radical models valid for radicals T1 and T2/T3, respectively.[9,8] Very few accurate **g** tensors are available in the literature for carbon-centered radicals in sugars, for which also the radical model is well-established. One might thus consider the stable radicals in sucrose as benchmark systems for DFT calculations of **g** tensors on this class of substances. The overall agreement of the calculated **g** tensors with those we experimentally determined is remarkably good. Considering first the principal values, the DFT results underestimate the absolute values of δg by about 15%, resulting in a computed isotropic shift and axiality smaller than the experimental values found in this work. The rhombicity and principal directions of the experimental tensors, on the other hand, are very well reproduced by the calculations.

C. Single Crystal EPR Spectrum Simulations. In Figure 4 the EPR spectra in the $\langle a^* \rangle$, $\langle b \rangle$, and $\langle c \rangle$ orientations, recorded at 110 K, low microwave power (<10 μW), and low modulation frequencies (3 kHz) are compared to simulations including contributions of the three radicals. Although the EIE spectra can be reproduced very well by simulations (see Figures 3 and S1), the agreement for the EPR spectra is less good. The positions of resolved lines in the simulated spectra still correspond well with features in the experimental spectra, but the relative line intensities are not reproduced and certain lines in the experimental spectra have no counterpart in the simulations. A limited trial and error search for optimization indicated that the EPR line widths exhibit a weak anisotropy (best result line widths are given in the caption of Figure 4). It seems, however, doubtful that more extensive fitting of these parameters would considerably reduce the mismatch, which also prevents an accurate estimate of the relative contributions of the three radicals. Visual inspection of agreement between simulated and experimental spectra allowed us to determine that the (T2 + T3)/T1 intensity ratio ranges between 0.9 and 1.7 and the T2/T3 ratio between 1 and 3. Simulations using optimum ratios of (T2 + T3)/T1 = 1.2 and T2/T3 = 1.5 are shown in Figure 4, along with the calculated individual contributions of the three radical species in each orientation.

In view of the good reproduction of the EIE spectra, the discrepancies between simulated and experimental single crystal spectra EPR are rather unexpected. Although it is hard to exclude that the observed deviations are not in part instrumental or due to (small) crystal misalignments, it is clear that certain parts of the spectra (indicated with circles in Figure 4) cannot be covered by simulations with the radicals analyzed till now. This shows that still other radicals contribute to the EPR spectrum in a non-negligible way, in agreement with the results of earlier statistical decomposition studies of the EPR spectra of irradiated sucrose powder.[5]

In order to assess the temperature dependence of the spectra and the validity of the spin Hamiltonian parameters here determined for simulation of powder spectra at RT, the single crystal EPR spectra in the $\langle a^* \rangle$, $\langle b \rangle$, and $\langle c \rangle$ orientations (3 kHz modulation frequency and 90 μW power) have also been recorded at RT and are shown in the bottom line of Figure 4. The positions of the most prominent transitions (in the 1210−1215 mT range) hardly exhibit any shift, whereas the HF interactions seem to be slightly better resolved at RT. This suggests that neither the **g** nor the HF tensors of T1−T3 exhibit strong temperature dependence in this range.

D. Powder EPR Spectrum Simulations. In the following we concentrate on powder EPR spectra of irradiated sucrose, as these are the most relevant for applications in dosimetry and irradiation of sugar-containing foodstuffs. As the single crystal analysis was performed at Q-band microwave frequencies, we will first focus on this frequency band. Next, the X-band spectrum will be dealt with, because for applications the EPR spectra are most often recorded in this band. In these two bands, both the 110 K and the RT spectra are recorded and compared with the simulations. In view of the above-mentioned limited temperature dependence of the single-crystal EPR spectra, one may expect that knowledge of the spin Hamiltonian parameters of T1−T3 at 110 K also allows understanding the powder EPR spectrum at RT, which is most relevant for applications. We have also simulated the powder spectra in higher microwave frequency bands, in which spectra have previously been recorded.[6] As we have no direct access to these spectra, the latter simulations are given in the Supporting Information (Figure S2).

The **g** and HF tensors determined in our single crystal studies (section 3A) are used as fixed input parameters for the simulations. A large number of parameters ($\sim$ 20) could in principle still be varied in order to fit the simulated spectra to experiment: principal values and directions of an anisotropic line width tensor—resulting from natural line broadening, unresolved HF interactions, and/or strain in the g and HF parameters—line shapes for each radical, and the relative contributions of the three radicals. We have explicitly chosen not to fit these parameters. All simulations presented in this section have been performed assuming the same radical intensity ratios as for the single crystal simulations. Variations

dx.doi.org/10.1021/jp400053h | J. Phys. Chem. B XXXX, XXX, XXX−XXX

of the relative radical concentrations, that were not attempted here, may lead to slight further improvement of the agreement between experimental and simulated spectra and could result from differences in the crystal size, the radiation dose (rate), and postradiation history. The anisotropic line width parameters in the Q- and X-band simulations have been chosen to be proportional to those in the single crystal simulations, with the single proportionality factor (the same for the three radicals) being the only free parameter in the simulations, determined by visual inspection of the agreement between experimental and simulated spectra. For the Q-band simulation, the line width proportionality factor is found to be close to 1. The smaller factor necessary for the X-band simulations very probably indicates that part of the residual EPR line width is due to strain in the *g* values.

Parts a and b of Figure 5 show the Q-band and X-band spectra, respectively. They are organized in the same way: the top three spectra represent the simulations for the individual radical components, taking the anisotropy of their **g** tensors into account, and the fourth spectrum shows the weighed sum of these spectra. The fifth and sixth traces from the top display the experimental spectra at 110 K and RT, respectively. These spectra were recorded at low microwave power and low modulation frequency (see caption). Finally, the bottom traces show simulations ignoring the *g* anisotropy of the radicals, i.e. by taking the average *g* value of each radical as the isotropic *g* value in the simulations.

From the comparison of 110 K, RT, and simulated powder spectra, we conclude the following:

(1) Similarly as in the single crystal spectra, the main changes in the central part of the spectra between 110 K and RT appear to be that the HF structure is better resolved at RT.

(2) The simulations including *g* anisotropy reproduce the experimental spectra, both at 110 K and at RT, quite well, especially considering that only one parameter has been optimized. Hence, knowledge of the spin Hamiltonian parameters of the dominant stable radicals in irradiated sucrose does allow understanding the essential characteristics of its powder EPR spectra.

(3) Knowledge of the **g** tensor for these radicals, with delocalization of spin density onto (carbonyl and ring) oxygen atoms, is essential in the powder EPR simulations. Ignoring the *g* anisotropy leads to an obvious mismatch at Q-band but, perhaps more surprisingly, even at X-band microwave frequencies, important for dosimetry applications. Simulations at higher frequencies (see Supporting Information, Figure S2) show that the basic characteristics of the stable high-field EPR spectra of irradiated sucrose may also be understood using the **g** tensors deduced in this work, keeping, of course, in mind the limited accuracy of their principal values, determined at 34 GHz.

(4) In the wings of the X- and Q-band EPR spectra, clear evidence is seen of as-yet unidentified radical components. These, most probably, also have a non-negligible contribution to the central part of the EPR spectra. A deeper understanding of these extra components should allow a considerably better reproduction of the complete EPR spectrum of irradiated sucrose and an accurate quantification of the relative radical contributions. This presents a strong motivation for characterizing and structurally identifying these components, combining ENDOR and EIE spectroscopy with DFT calculations. The study of these radicals falls outside the scope of the present paper, however.

4. CONCLUSIONS

We determined the **g** tensors for the three stable radical species that dominate the EPR spectrum of irradiated sucrose, from angular dependent EIE measurements at 110 K on single crystals. On the basis of the very good reproduction of the single crystal EIE spectra, we are confident that the principal values and directions, axiality and rhombicity of these tensors are more reliable than those published earlier. The accuracy of the principal values is, of course, limited by the microwave frequency at which the study was performed and single crystals studies at higher frequencies may further improve these. DFT calculated **g** tensors for the previously established models for these radicals are in the best agreement one may expect (principal *g* values within roughly 15%) with the tensors we determined here, the agreement in principal directions even being excellent. Simulations at X- and Q-band frequencies reproduce the experimental powder EPR spectra recorded at 110 K and RT fairly well, especially considering the fact that only one line width parameter was optimized and that non-negligible radical contributions, clearly evident in the wings of the spectra, but also influencing the shape of the central part, are not taken into account. Knowledge of the spin Hamiltonian parameters of the radicals T1−T3 does allow understanding of the main characteristics of the dosimetric sucrose EPR spectrum. This motivates a thorough spectroscopic and DFT study of the still unidentified components in order to understand this dosimetric spectrum fully. The present study has shown that the **g** tensor information is crucial for obtaining reliable powder EPR simulations of these radicals, even at the low X-band microwave frequencies. From a more general perspective, we also demonstrated that when using literature spin Hamiltonian data for simulating angular dependent single crystal and powder EPR spectra of radicals in similar systems, it is important to bear Schonland and radical site ambiguities in mind.

■ ASSOCIATED CONTENT

Supporting Information

g and hyperfine tensors, all referring to the same radical site, for T1−T3, used in the single crystal EPR simulations in Figures 3−7 and S1. Experimental EIE and simulated EPR spectra for radicals T1−T3 as a function of rotation angle in three rotation planes. Simulation of the powder EPR spectrum of irradiated sucrose at 94, 190, and 285 GHz. This material is available free of charge via the Internet at http://pubs.acs.org.

■ AUTHOR INFORMATION

Corresponding Author

*E-mail: Henk.Vrielinck@UGent.be. Telephone: +32 9 264 4356. Fax: +32 0 264 4996.

Notes

The authors declare no competing financial interest.

■ ACKNOWLEDGMENTS

The authors thank the Research Foundation Flanders (FWO-Vlaanderen) for financial support. H.D.C. acknowledges a Postdoctoral Fellowship with the same organization. A.V.Y.-

D.D. acknowledges a Ph.D. scholarship of the Research Board of Ghent University. The computational resources and services used were provided by Ghent University (Stevin Supercomputer Infrastructure).

REFERENCES

(1) Shields, H.; Hamrick, P. X-Irradiation Damage of Sucrose Single Crystal. *J. Chem. Phys.* **1962**, *37*, 202−203.
(2) Lomaglio, G. Résonance Paramagnétique Electronique et Susceptibilité Paramagnétique d'un Monocristal de Saccharose Irradié. *C. R. Seances Acad. Sci., Ser. B* **1967**, *264*, 1637.
(3) Gräslund, A.; Löfroth, G. Free-Radicals in Gamma-Irradiated Single-Crystals of Trehalose Dihydrate and Sucrose Studied by Eelectron-Paramagnetic Resonance. *Acta Chem. Scand., Ser. B* **1975**, *29*, 475−482.
(4) Sagstuen, E.; Lund, A.; Awadelkarim, O.; Lindgren, M.; Westerling, J. Free-Radicals in X-Irradiated Single-Crystals of Sucrose—A Reexamination. *J. Phys. Chem.* **1986**, *90*, 5584−5588.
(5) Vanhaelewyn, G.; Sadlo, J.; Callens, F.; Mondelaers, W.; De Frenne, D.; Matthys, P. A Decomposition Study of the EPR Spectrum of Irradiated Sucrose. *Appl. Radiat. Isot.* **2000**, *52*, 1221−1227.
(6) Georgieva, E. R.; Pardi, L.; Jeschke, G.; Gatteschi, D.; Sorace, L.; Yordanov, N. D. High-Field/High-Frequency EPR Study on Stable Free Radicals Formed in Sucrose by Gamma-Irradiation. *Free Radical Res.* **2006**, *40*, 553−563.
(7) De Cooman, H.; Pauwels, E.; Vrielinck, H.; Dimitrova, A.; Yordanov, N. D.; Sagstuen, E.; Waroquier, M.; Callens, F. Radiation-Induced Defects in Sucrose Single Crystals, Revisited: A Combined Electron Magnetic Resonance and Density Functional Theory Study. *Spectrochim. Acta A* **2008**, *69*, 1372−1383.
(8) De Cooman, H.; Pauwels, E.; Vrielinck, H.; Sagstuen, E.; Callens, F.; Waroquier, M. Identification and Conformational Study of Stable Radiation-Induced Defects in Sucrose Single Crystals Using Density Functional Theory Calculations of Electron Magnetic Resonance Parameters. *J. Phys. Chem. B* **2008**, *112*, 7298−7307.
(9) De Cooman, H.; Pauwels, E.; Vrielinck, H.; Sagstuen, E.; Van Doorslaer, S.; Callens, F.; Waroquier, M. ENDOR and HYSCORE Analysis and DFT-Assisted Identification of the Third Major Stable Radical in Sucrose Single Crystals X-Irradiated at Room Temperature. *Phys. Chem. Chem. Phys.* **2009**, *11*, 1105−1114.
(10) De Cooman, H.; Pauwels, E.; Vrielinck, H.; Sagstuen, E.; Waroquier, M.; Callens, F. Oxidation and Reduction Products of X Irradiation at 10 K in Sucrose Single Crystals: Radical Identification by EPR, ENDOR, and DFT. *J. Phys. Chem. B* **2010**, *114*, 666−674.
(11) De Cooman, H.; Vanhaelewyn, G.; Pauwels, E.; Sagstuen, E.; Waroquier, M.; Callens, F. Radiation-Induced Radicals in Glucose-1-phosphate. I. Electron Paramagnetic Resonance and Electron Nuclear Double Resonance Analysis of in situ X-Irradiated Single Crystals at 77 K. *J. Phys. Chem. B* **2009**, *112*, 15045−15053.
(12) Pauwels, E.; De Cooman, H.; Vanhaelewyn, G.; Sagstuen, E.; Callens, F.; Waroquier, M. Radiation-Induced Radicals in Glucose-1-phosphate. II. DFT Analysis of Structures and Possible Formation Mechanisms. *J. Phys. Chem. B* **2009**, *112*, 15054−15063.
(13) Von Sonntag, C. *Free-radical-induced DNA damage and its repair—A chemical perspective*; Springer-Verlag: Berlin, 2006.
(14) Nakajima, T. Sugar as an Emergency Populace Dosimeter for Radiation Accidents. *Health Phys.* **1988**, *55*, 951−955.
(15) Nakajima, T. Possibility of Retrospective Dosimetry for Persons Accidentally Exposed to Ionizing-Radiation Using Electron-Spin Resonance of Sugar and Mother-of-Pearl. *Br. J. Radiol.* **1989**, *62*, 148−153.
(16) Silveira, F. A. M.; Baffa, O. Lyoluminescence and ESR Measurements on Alanine and Sucrose Dosimeters. *Appl. Radiat. Isot.* **1995**, *46*, 827−830.
(17) Son, P. K.; Ok, C. I.; Kim, J. W. EPR Study of Sugar Irradiated with X-Rays. *J. Korean Phys. Soc.* **2001**, *38*, 315−317.
(18) Yordanov, N. D.; Gancheva, V.; Georgieva, E. EPR and UV Spectroscopic Study of Table Sugar as a High-Dose Dosimeter. *Radiat. Phys. Chem.* **2002**, *65*, 269−276.
(19) Yordanov, N. D.; Georgieva, E. EPR and UV Spectral Study of Gamma-Irradiated White and Burned Sugar, Fructose and Glucose. *Spectrochim. Acta A* **2004**, *60*, 1307−1314.
(20) Desrosiers, M.; Wadley, S. Time Dependence of the Radiation-Induced EPR Signal in Sucrose. *Radiat. Prot. Dosim.* **2006**, *118*, 479−481.
(21) Trompier, F.; Bassinet, C.; Wieser, A.; De Angelis, C.; Viscomi, D.; Fattibene, P. Radiation-Induced Signals Analysed by EPR Spectrometry Applied to Fortuitous Dosimetry. *Ann. Ist. Super. Sanita* **2009**, *45*, 287−296.
(22) Karakirova, Y.; Yordanov, N. D.; De Cooman, H.; Vrielinck, H.; Callens, F. Dosimetric Characteristics of Different Types of Saccharides: An EPR and UV Spectrometric Study. *Radiat. Phys. Chem.* **2010**, *79*, 654−659.
(23) Vrielinck, H.; De Cooman, H.; Karakirova, Y.; Yordanov, N. D.; Callens, F. Early-Stage Evolution of the EPR Spectrum of Crystalline Sucrose at Room Temperature after High-Dose X Irradiation. *Radiat. Res.* **2009**, *172*, 226−233.
(24) Helle, N.; Linke, B.; Magern, M.; Schreiber, G.; Bogl, K. W. Evaluation of the Electron-Spin-Resonance Technique for the Detection of Irradiated Foofstuffs. *Z. Ernaehrungswiss.* **1992**, *31*, 205−218.
(25) Raffi, J.; Stevenson, M. H.; Kent, M.; Thiery, J. M.; Belliardo, J.-J. European Intercomparison on Electron-Spin-Resonance Identification of Irradiated Foodstuffs. *Int. J. Food Sci. Technol.* **1992**, *27*, 111−124.
(26) Desrosiers, M. F. Current Status of the EPR Method to Detect Irradiated Food. *Appl. Radiat. Isot.* **1996**, *47*, 1621−1628.
(27) Yordanov, N. D.; Pachova, Z. Gamma-Irradiated Dry Fruits—An Example of a Wide Variety of Long-Time Dependent EPR Spectra. *Spectrochim. Acta A* **2006**, *63*, 891−895.
(28) Spaeth, J.-M.; Niklas, J. R.; Bartram, R. H. *Structural analysis of point defects in solids—An introduction to multiple magnetic resonance spectroscopy*; Springer-Verlag: Berlin-Heidelberg, 1992.
(29) Kang, J.; Tokdemir, S.; Shao, J.; Nelson, W. H. Electronic g-Factor Measurement from ENDOR-Induced EPR Patterns: Malonic Acid and Guanine Hydrochloride Dehydrate. *J. Magn. Reson.* **2003**, *165*, 128−136.
(30) Brown, G. M.; Levy, H. A. Further Refinement of Structure of Sucrose Based on Neutron-Diffraction Data. *Acta Crystallogr., Sect. B: Struct. Sci.* **1973**, *29*, 790−797.
(31) Serway, R. A.; Marshall, S. A. Electron Spin Resonance Absorption Spectra of CO_3^- and CO_3^{3-} Molecule-Ions in Irradiated Single-Crystal Calcite. *J. Chem. Phys.* **1967**, *46*, 1949−1952.
(32) Stoll, S.; Schweiger, A. EasySpin, a Comprehensive Software Package for Spectral Simulation and Analysis in EPR. *J. Magn. Reson.* **2006**, *178*, 42−55.
(33) Lippert, G.; Hutter, J.; Parrinello, M. A Hybrid Gaussian and Plane Wave Density Functional Scheme. *Mol. Phys.* **1997**, *92*, 477−487.
(34) VandeVondele, J.; Krack, M.; Mohamed, F.; Parinello, M.; Chassaing, T.; Hutter, J. QUICKSTEP: Fast and Accurate Density Functional Calculations Using a Mixed Gaussian and Plane Waves Approach. *Comput. Phys. Commun.* **2005**, *167*, 103−128.
(35) Goedecker, S.; Teter, M.; Hutter, J. Separable Dual-Space Gaussian Pseudopotentials. *Phys. Rev. B* **1996**, *54*, 1703−1710.
(36) Hartwigsen, C.; Goedecker, S.; Hutter, J. Relativistic Separable Dual-Space Gaussian Pseudopotentials from H to Rn. *J. Phys. Rev. B* **1998**, *58*, 3641−3662.
(37) Lippert, G.; Hutter, J.; Parrinello, M. The Gaussian and Augmented-Plane-Wave Density Functional Method for Ab Initio Molecular Dynamics Simulations. *Theor. Chem. Acc.* **1999**, *103*, 124−140.
(38) Krishnan, R.; Binkley, J. S.; Seeger, R.; Pople, J. A. Self-Consistent Molecular-Orbital Methods 0.20. Basis Set for Correlated Wave-Functions. *J. Chem. Phys.* **1980**, *72*, 650−654.

(39) Weber, V.; Iannuzzi, M.; Giani, S.; Hutter, J.; Declerck, R.; Waroquier, M. Magnetic Linear Response Properties Calculations with the Gaussian and Augmented-Plane-Wave Method. *J. Chem. Phys.* **2009**, *131*, No. 014106.
(40) Declerck, R.; Van Speybroeck, V.; Waroquier, M. First-Principles Calculations of Hyperfine Parameters with the Gaussian and Augmented-Plane-Wave Method: Application to Radicals Embedded in a Crystalline Environment. *Phys. Rev. B* **2006**, *74*, No. 245103.
(41) Becke, A. D. Density-Functional Exchange-Energy Approximation with Correct Asymptotic-Behavior. *Phys. Rev. A* **1988**, *38*, 3098−3100.
(42) Lee, C.; Yang, W.; Parr, R. Development of the Colle-Salvetti Correlation-Energy Formula into a Functional of the Electron-Density. *Phys. Rev. B* **1988**, *37*, 785−789.
(43) Pauwels, E.; Asher, J.; Kaupp, M.; Waroquier, M. Cluster or Periodic, Static or Dynamic-the Challenge of Calculating the g Tensor of the Solid-State Glycine Radical. *Phys. Chem. Chem. Phys.* **2011**, *13*, 18638−18646.
(44) Neese, F. Efficient and Accurate Approximations to the Molecular Spin-Orbit Coupling Operator and their Use in Molecular g-Tensor Calculations. *J. Chem. Phys.* **2005**, *122*, No. 034107.
(45) Van Yperen-De Deyne, A.; Pauwels, E.; Van Speybroeck, V.; Waroquier, M. Accurate Spin-Orbit and Spin-Other-Orbit Contributions to the g-Tensor for Transition Metal Containing Systems. *Phys. Chem. Chem. Phys.* **2012**, *14*, 10690−10704.
(46) Schreckenbach, G.; Ziegler, T. Calculation of the g-Tensor of Electron Paramagnetic Resonance Spectroscopy using Gauge-Including Atomic Orbitals and Density Functional Theory. *J. Phys. Chem. A* **1997**, *101*, 3388−3399.
(47) Kaupp, M.; Reviakine, R.; Malkina, O. L.; Arbuznikov, A.; Schimmelpfennig, B.; Malkin, V. G. Calculation of Electronic g-Tensors for Transition Metal Complexes Using Hybrid Density Functionals and Atomic Meanfield Spin-Orbit Operators. *J. Comput. Chem.* **2002**, *23*, 794−803.
(48) Malkin, V. G.; Malkina, O. L.; Reviakine, R.; Arbouznikov, A. V.; Kaupp, M.; Schimmelpfennig, B.; Malkin, I.; Helgaker, T.; Ruud, K. MAG-Respect, Version 1.2 (2003).
(49) Tarpan, M. A.; Vrielinck, H.; De Cooman, H.; Callens, F. Determination of the g Tensors for the Dominant Stable Radicals in X-Irradiated beta-D-Fructose Single Crystals. *J. Phys. Chem. A* **2009**, *113*, 7994−8000.
(50) Kaupp, M.; Remenyi, C.; Vaara, J.; Malkina, O. L.; Malkin, V. G. Density Functional Calculations of Electronic g-Tensors for Semiquinone Radical Anions. The Role of Hydrogen Bonding and Substituent Effects. *J. Am. Chem. Soc.* **2002**, *124*, 2709−2722.
(51) Jeschke, G. EPR Techniques for Studying Radical Enzymes. *Biochim. Biophys. Acta* **2005**, *1707*, 91−102.
(52) Un, S. The g-Values and Hyperfine Coupling of Amino Acid Radicals in Proteins: Comparison of Experimental Measurements with Ab Initio Calculations. *Magn. Reson. Chem.* **2005**, *43*, S229−S236.
(53) Svistunenko, D. A.; Jones, G. A. Tyrosyl Radicals in Proteins: A Comparison of Empirical and Density Functional Calculated EPR Parameters. *Phys. Chem. Chem. Phys.* **2009**, *11*, 6600−6613.
(54) Schonland, D. S. On the Determination of the Principal g-Values in Electron Spin Resonance. *Proc. Phys. Soc. London* **1959**, *73*, 788−792.
(55) Vrielinck, H.; De Cooman, H.; Tarpan, M. A.; Sagstuen, E.; Waroquier, M.; Callens, F. Schonland Ambiguity in the Electron Nuclear Double Resonance Analysis of Hyperfine Interactions: Principles and Practice. *J. Magn. Reson.* **2008**, *195*, 196−205.